Chirality-Dependent Amino Acid Modulation of RNA Folding

David A. Nicholson, Abhigyan Sengupta, and David J. Nesbitt*

Cite This: https://dx.doi.org/10.1021/acs.jpcb.0c07420

Read Online

ACCESS | Metrics & More | Article Recommendations | Supporting Information

ABSTRACT: The preponderance of a specific D- or L-chirality in fats, sugars, amino acids, nucleic acids, and so on is ubiquitous in nature, yet the biological origin of such chiral dominance (i.e., with one enantiomer overwhelmingly present) remains an open question. One plausible proposal for the predominance of L-chirality in amino acids could be through evolutionary templating of chiral RNA-folding via chaperone activity. To help evaluate this possibility, single molecule fluorescence experiments have been performed that measure the chiral dependence of chaperone folding dynamics for the simple tetraloop−tetraloop receptor (TL-TLR) tertiary binding motif in the presence of a series of chiral amino acids. Specifically, D- vs L-arginine is found to accelerate the unfolding of this RNA motif in a chirally selective fashion, with temperature-dependent studies of the kinetics performed to extract free energy, enthalpy, and entropy landscapes for the underlying thermodynamics. Furthermore, all-atom molecular dynamics (MD) simulations are pursued to provide additional physical insight into this chiral sensitivity, which reveal enantiomer-specific sampling of nucleic acid surfaces by D- vs L-arginine and support a putative mechanism for chirally specific denaturation of RNA tertiary structure by arginine but not other amino acids.
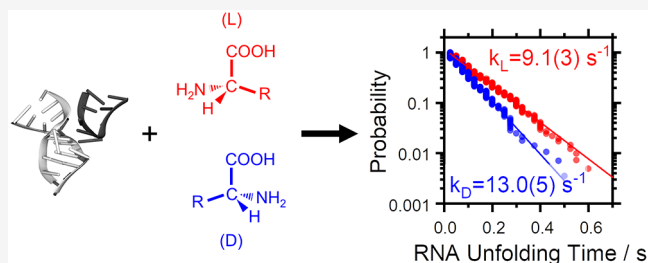
I. INTRODUCTION

From the overwhelming abundance of homochiral species in nature, it appears that biology abhors racemic mixtures. The tendency toward homochirality (or chiral purity) is a long appreciated hallmark of biological systems,[1] characterizing the biosynthesis of proteins, nucleic acids, saccharides, and small molecules.[2,3] Consider the case of homochirality in proteins, for which all amino acids more complex than glycine have chiral centers, yet biology almost exclusively favors L-amino acids.[4,5] This remarkable evolution toward homochirality in proteins, for example, demands to be accounted for in any complete model of the origin of life, for which a number of mechanisms have been proposed. One family of theories suggests that homochirality initially developed in nucleic acids during the RNA world[6] and was subsequently transmitted to amino acids. For instance, protein synthesis in a D-ribose RNA world could have an inherent bias toward L-amino acids, as demonstrated in the chiral discrimination of amino acids during uncatalyzed aminoacylation of tRNA, a key step in protein synthesis.[7,8]

An alternative possibility explored herein is that evolutionary selection of amino acid chirality occurred *before* the development of protein synthesis, based instead on the role of amino acids in the RNA world, possibly as nucleic acid-folding chaperones.[9,10] RNA molecules are notoriously inefficient at folding into biologically competent form,[11] with slow folding kinetics and therefore a tendency to adopt long-lived misfolded states (with lifetimes of order 1−1000 s).[10] Modern biology in the current proteomic era addresses such issues through the use of proteins[12] as well as osmolytes[13] as chaperones to guide the pathway toward correct RNA folding. It is thus entirely reasonable to expect that early life would explore similar strategies, utilizing amino acids as small molecule chaperones. Indeed, experiments have recently demonstrated the ability of amino acids to influence RNA folding at secondary[14] and tertiary[15] structure levels (and at even higher ribozyme[16] levels of complexity) at 10−100 mM concentrations (1 mM = 1 mmol/L). Although the corresponding affinities are relatively low, such concentrations are well within the limits of osmolyte cellular levels, which can be in excess of 1 M.[17,18] If early life relied on amino acids to modulate the thermodynamic stability and/or kinetics of RNA folding and if the capacity of amino acids to chaperone RNA folding depends on amino acid chirality, then the resulting evolutionary pressure could have promoted an amino acid synthesis mechanism that favors the now ubiquitous L-amino acid.

This is a bold statement, requiring experimental evidence to evaluate as even a putative evolutionary pathway. Many studies on the chiral dependence of amino acid−nucleic acid interactions have focused on aminoacylation of tRNA structures, with a sizable body of work established.[7,8,19,20] Amino acid chirality effects have also been examined in other contexts, such as codon binding,[21−23] histidine selection,[24] chromatographic applications,[25,26] and ribozyme activity.[27] Indeed, the study of Yarus and Majerfeld represents an especially intriguing and relevant case in point, in which they identified an arginine-specific binding pocket in the *Tetrahymena* ribozyme that exhibited a 10-fold higher selectivity for L-arginine over D-arginine, with clear catalytic implications. These ensemble studies provided substantial first insights into how nucleic acid structures might sense amino acid chirality. However, few experiments have been performed at the single molecule level, which can in principle provide even deeper levels of physical understanding into a mechanism for chirally sensitive RNA folding.[28]

In a previous work, we reported[14] on single-molecule experiments investigating the effects of amino acids on nucleic acid *secondary* structure folding kinetics, for which no dependence on amino acid chirality was observed. We have also examined[15] how the presence of amino acids can influence the formation of RNA *tertiary* structure, for which significant chaperone effects were indeed observed but without further exploration into any dependence on amino acid chirality. To test for such chiral chaperone effects, an additional stratum of work is necessary, specifically, a single molecule study into chiral amino acid influence on chiral RNA tertiary folding, which represents the focus of the present paper.

Here, we utilize single molecule methods in a search for amino acid chiral dependency on RNA tertiary folding dynamics. Specifically, we explore the ubiquitous 11-nt GAAA tetraloop−tetraloop receptor (TL-TLR) motif[29] as a model tertiary folding system, exploiting single molecule fluorescence resonance energy transfer (smFRET) to probe conformational changes in the RNA construct. Rate constants for TL-TLR folding (k_{fold}) and unfolding (k_{unfold}) are systematically investigated for a series of enantiomeric pairs over a wide range of amino acid concentrations. Interestingly, we observe a strong chiral dependence for D- and L-arginine inhibition of RNA TL-TLR tertiary folding and yet no evidence of a similar chirally sensitive signature for any other chiral species selected from five representative classes of soluble amino acids (lysine, histidine, alanine, serine, and proline). In addition, single molecule folding studies of these amino acid−RNA constructs are explored under temperature-controlled conditions in order to extract both chirally sensitive and chirally insensitive enthalpic and entropic contributions to the folding free energy landscape. Finally, these single molecule experiments are complemented by all-atom molecular dynamics (MD) simulations in efforts to provide additional insight and microscopic perspective into the chiral dependence of the amino acid-assisted folding and unfolding kinetics.

II. METHODS

RNA FRET Construct. To examine the influence of amino acid chirality in modulating RNA tertiary folding, we employ an RNA construct bearing an isolated tetraloop−tetraloop receptor (TL-TLR) folding motif (Figure 1), which has been successfully used in previous studies to examine various kinetic and thermodynamic aspects of TL-TLR folding at the single
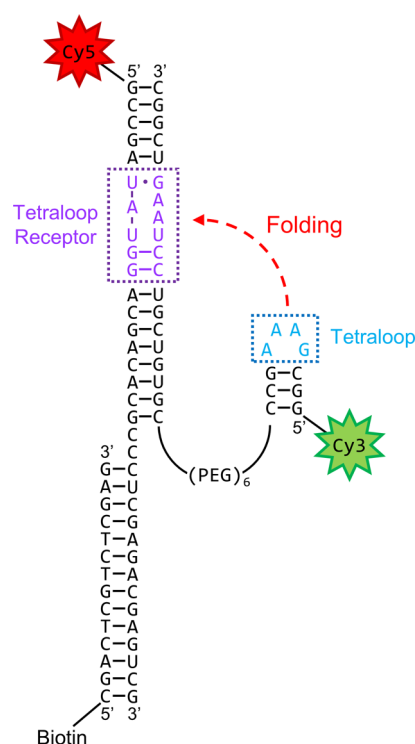

Figure 1. Structure of the 3-stranded TL-TLR smFRET construct.

molecule level.[15,29,30] The construct consists of three strands: (1) a biotinylated DNA oligonucleotide for surface attachment (5′-biotin-CGACTCGTCTCGAG-3′), (2) an RNA sequence labeled with cyanine 5 (Cy5) at the 5′-position (5′-Cy5-GCCGAUAUGGACGACACGCCCUCGAGACGAGUCG-3′), and (3) an RNA strand containing a GAAA tetraloop, an internal hexameric poly(ethylene glycol) (PEG) linkage, and a cyanine 3 (Cy3) fluorophore at the 5′-terminus (5′-Cy3-GGCGAAGCC-PEG$_6$-CGUGUCGUCCUAAGUCGGC-3′). All sequences are commercially synthesized and HPLC-purified (Integrated DNA Technologies), where companies/sources identified herein do not indicate product support. Strands 1 and 2 hybridize to form a stable 14-base-pair RNA−DNA duplex, while strands 2 and 3 bind to generate the tetraloop receptor (TLR) domain flanked by double helices to help maintain structural stability (see Figure 1). The flexible PEG linker in strand 3 largely avoids potential persistence length issues due to base-stacking in an ssRNA linker, which could in turn hinder diffusion of the GAAA tetraloop.[31] The strands are annealed by heating a 10 μmol/L mixture to 85 °C, slowly cooling to room temperature at 1 °C/min, prior to long-term storage at −20 °C. The annealed stock is used without purification, since constructs lacking the biotinylated strand do not attach to the surface and constructs lacking the Cy3-labeled strand are not excited by the laser ($\sigma_{\text{Cy5}}/\sigma_{\text{Cy3}}$ = 3% at 532 nm).

Sample Preparation. Samples are prepared in a home-configured glass flow cell, for which a #1.5 glass coverslip (CGI Life Sciences) is soaked overnight in acetone and cleaned in a UV-ozone oven (Jelight Mo. 42) for 30 min. The clean coverslip is attached to a glass slide (VWR) by two parallel strips of double-sided tape, forming a channel approximately 2 mm wide, 22 mm long, and 0.1 mm deep to act as a flow cell for rapid solution exchange. The coverslip surface is labeled with the RNA FRET construct by using biotin−streptavidin

interactions, as previously described.[15,32,33] Three solutions, all buffered with 50 mM HEPES at pH 7.6, are sequentially incubated in the sample chamber for 10 min in the following order: (i) 10 mg/mL bovine serum albumin (BSA) with 1 mg/mL biotinylated-BSA to block and biotinylate the glass surface, (ii) 0.2 mg/mL streptavidin to bind the biotin with streptavidin tetramers, and (iii) 1 nM biotinylated TL-TLR construct to bind to the streptavidin, resulting in a surface RNA coverage of ~0.1/μm^2. For each experiment, the sample chamber is washed with buffer prior to filling with an imaging solution consisting of a buffer (50 mM HEPES, pH 7.6), an oxygen scavenging cocktail[34] (100 nM protocatechuate 3,4-dioxygenase, 5 mM protocatechuic acid in equimolar sodium hydroxide, and 2 mM Trolox), a metal chelating agent (0.1 mM EDTA), monovalent salt (50 mM KCl; total [M$^+$] = 80 mM), and the desired D/L-amino acid (see results: note that arginine and lysine are added as chloride salts to maintain near neutral pH). HEPES has been purchased from MP Biomedicals, EDTA and L-histidine are from Fluka, D-histidine and L-serine are from Alfa Aesar, and D-alanine and D-proline are from Fischer, with all other compounds obtained from Sigma-Aldrich.

Single-Molecule Instrumentation. Single-molecule measurements are carried out by total internal reflection fluorescence (TIRF) microscopy (schematically outlined in Figure 2), with a similar design to other through-objective TIRF microscopes.[35] Light from a 532 nm diode-pumped solid-state laser (MeshTel GSF32−300PS) is directed into an inverted microscope (Zeiss Axiovert 135) where it is focused

Figure 2. (a) TIRF instrument schematic. 532 nm light is focused by lens L1 onto the back focal plane of the microscope objective. Emission collected by the objective passes through dichroic mirror DM1 to remove excitation light and is spatially filtered by a 1.5 mm slit placed at the focus of the tube lens L2. Cy3 and Cy5 emission are separated and recombined as offset images by dichroic mirrors DM2 and DM3. In addition, the images are magnified by a 4× telescope (L3: L4/L4′) before detection by a CCD camera.

onto the back focal plane of a 1.4 NA, oil-immersion microscope objective (Olympus PLAPON60XOSC2; Olympus Type-F immersion oil). To achieve total internal reflection, moving a mirror translates the beam laterally away from the optical axis, thereby increasing angle of incidence at the sample until the critical angle is reached. Fluorescence from the sample is collected by the same objective before passing through a 550 nm LP dichroic mirror (Chroma) to filter out reflected and scattered excitation light, with the transmitted photons collected on a charge-coupled device (CCD) video camera. First, Cy3 and Cy5 fluorescence is separated into two channels by a 645 nm LP dichroic mirror (Chroma DRLP), which are recombined by a second dichroic mirror to laterally offset the two images and project them side-by-side onto the CCD. Second, the images are magnified by a 4× telescope, with Cy3 and Cy5 emission focused independently using separate lenses (L4 and L4′) to reduce chromatic aberration. Finally, the emission is transmitted through an ~1.5 mm slit placed at the focus of the microscope's tube lens, truncating the circular image to maximize use of the CCD's square imaging area. Light is detected and recorded as grayscale movies by an intensified CCD camera (Princeton Instruments I-PentaMAX 512-EFT) with on-chip 3 × 3 pixel binning to increase the acquisition framerate to 40 Hz.

Data Analysis. Single-molecule movies are analyzed by using custom analysis software written in LabWindows/CVI (National Instruments). The first ~100 frames of each movie are averaged to smooth over conformational fluctuations, and local thresholding is applied to the averaged image to locate particles, whose (x, y) centroid positions are then refined by 2D Gaussian fitting. Summation over a 4 pixel diameter circle yields single particle fluorescence traces as a function of time, which are converted to actual photon count rates with calibration factors obtained from the variance-mean ratio method.[36] Single molecule trajectories are sorted into donors and acceptors by lateral position on the CCD camera, with donor−acceptor pairs identified by calibrated affine mapping.[37] Subsequent FRET data analysis follows protocols we have used in previous studies:[38] donor and acceptor fluorescence traces are combined into single-molecule FRET (smFRET) trajectories, from which state-to-state transition times are extracted by thresholding. Cumulative dwell time distributions are then subjected to single-exponential least-squares fit analysis, thereby yielding rate constants for both folding and unfolding of the single molecule constructs.

Temperature Control. Temperature control is established by using dual thermoelectric coolers (TEC), depicted in Figure 3, in which two TECs (upper and lower) are used as a distributed source of cooling to minimize thermal gradients across the sample. TEC modules (TE Technology HP-127-1.0-0.8) are compression-mounted between aluminum plates and coupled to the sample via thermal pads (EN-Laboratories). The upper TEC assembly lies directly on top of the sample slide, while the lower one embraces the microscope objective, which is in thermal contact with the sample through the immersion oil. Precise temperature stabilization (±0.05 °C, τ < 1 min response time, Figure 3c) is achieved via digital servo loop control. Specifically, sample and objective temperatures are measured by thermistors (Vishay) which feed into bidirectional temperature controllers (TE Technology TC-720) that drive the upper and lower TEC modules, respectively. The upper operational temperature of the system (~40 °C) is constrained by softening of optical cement in the
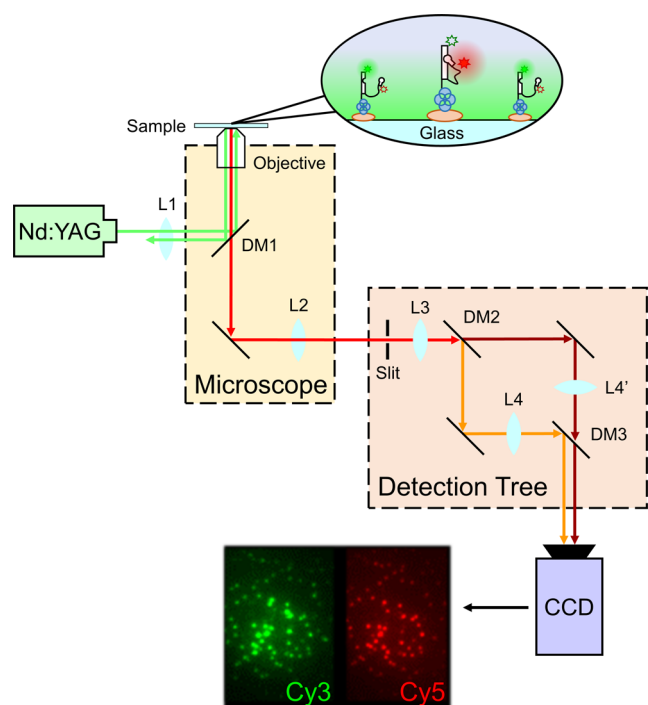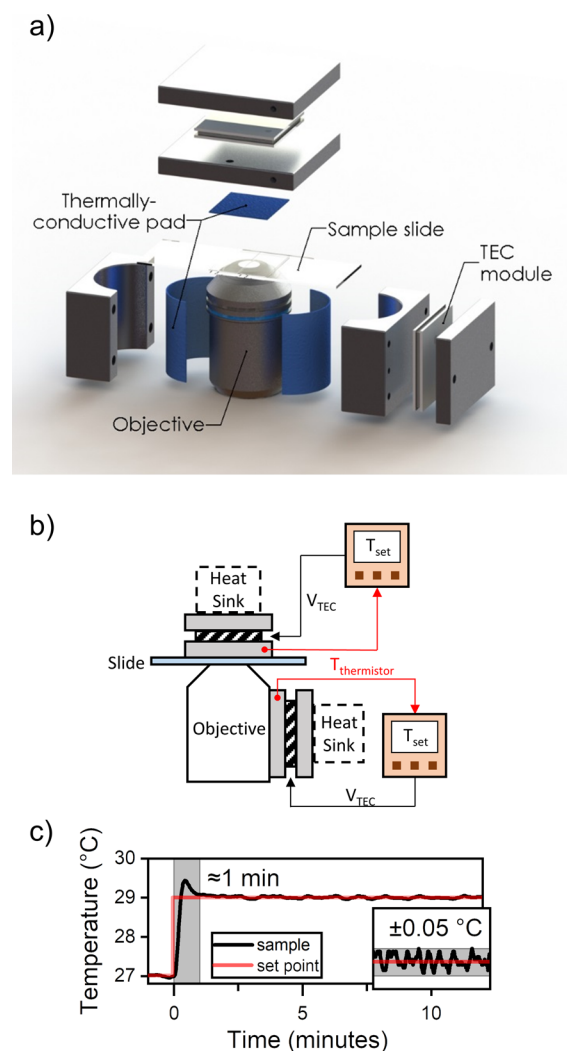
Figure 3. Temperature control apparatus. (a) To minimize thermal gradients, the sample is contacted by two TEC assemblies: one directly on the glass slide and the other mediated by the microscope objective. (b) Schematic of TEC control system. (c) Sample response time and temperature stability (inset) of the TEC system.

microscope objective at ~45 °C, while the lowest temperature is limited by air cooling efficiency to the heat sink. The coldest temperature data reported herein (~10 °C) required supplemental cooling of the TEC heat sink by contact with an enclosed frozen liquid reservoir (e.g., ice).

Molecular Dynamics Simulations. To complement these smFRET experimental results, we have in parallel pursued all-atom molecular dynamics (MD) simulations with explicit solvent. Initial structures for the nucleic acid constructs are used directly from the protein database (PDB), with the exception of the docked TL-TLR (PDB 1GID), which is truncated to residues belonging to the tetraloop (TL) and tetraloop receptor (TLR) residue indices (148−155, 220−229, and 245−253) to reduce system size. In the AmberTools19 software suite,[39] the three structures of interest (TL, TLR, and TL-TLR) are each solvated in a 15 Å padded TIP3P water box,[40] for which the total charge is neutralized by K^+ ions and with an additional 150 mM KCl to mimic the experimental ionic strength. Amino acids are added as chloride salts by using the Visual Molecular Dynamics (VMD)[41] software package, with initial positions selected at random. Dynamics are based

on Amber force fields: χ_{OL3} for RNA,[42] Cheatham and Young's parameters for the ions,[43] the TIP3P model for water, and Horn's zwitterionic amino acid parametrization for D- and L-amino acids.[44] Simulations have been performed on the Nanoscale Molecular Dynamics (NAMD)[45] platform by using periodic boundary conditions and a 2 fs time step, made possible by the constraining NH, CH, and OH bonds as rigid. Constant-temperature and -pressure conditions are maintained by Langevin dynamics at 300 K (1 ps^{-1} damping rate), with a Berendsen barostat at 1 atm (100 fs relaxation time, 4.57 × 10^{-5} bar^{-1} compressibility) and simulation snapshots stored every 10 ps. All other parameters are initialized at NAMD default values, with VMD software used for simulation analysis and visualization.[46]

III. EXPERIMENTAL RESULTS

RNA Tertiary Folding Demonstrates a Strong Chiral Sensitivity to Arginine. Single molecule experiments have been performed to evaluate the ability of amino acids to promote or inhibit RNA tertiary folding in a chirally sensitive fashion. We select an RNA construct bearing a tetraloop−tetraloop receptor (TL-TLR) motif and a FRET fluorophore pair (Figure 1) as a representative tertiary folding system.[29,30] Surface-tethered TL-TLR molecules are observed in a TIRF microscope to monitor and extract the single molecule folding dynamics, with sample smFRET trajectories shown in Figure 4a. The trajectories demonstrate clear two-state behavior, with the two distinct FRET efficiencies $E_{low} \approx 0.4$ and $E_{high} \approx 0.7$ representing the TL-TLR unfolded and folded states, respectively.[30] Under control conditions (50 mM HEPES buffer, 80 mM M^+, pH 7.6), the TL-TLR construct favors the folded state ($K_{eq} = 2.9 \pm 0.2$, where the uncertainty represents
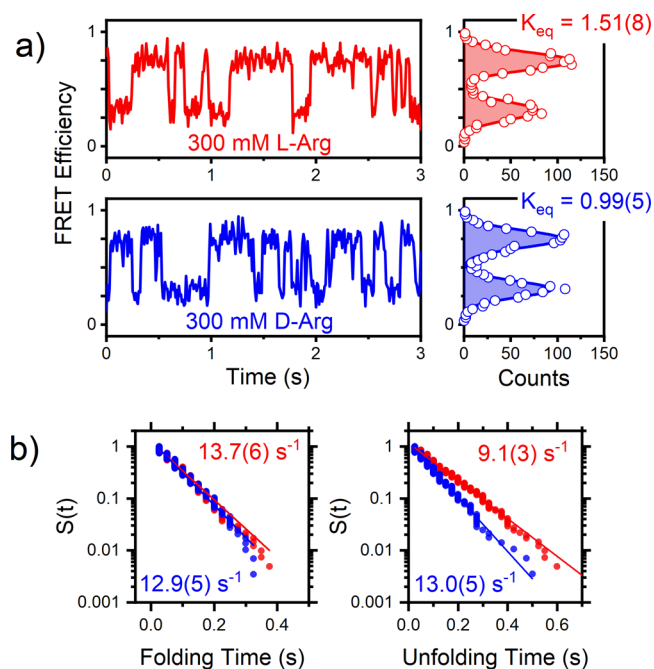

Figure 4. (a) Sample single-molecule TIRF trajectories for TL-TLR folding with 300 mM L-arginine (red, top row) and 300 mM D-arginine (blue, bottom row). FRET histograms with double Gaussian fits are shown to the right. (b) Survival functions for TL-TLR dwell times. Lines are single-exponential fits, from which rate constants can be extracted.

the standard deviation of the mean (σ_m)). Addition of 300 mM L-arginine (as L-arginine chloride) strongly *destabilizes* the folding equilibrium by nearly 2-fold (K_{eq} = 1.51 $\pm$ 0.08), in agreement with previous observations.[15] More relevantly to this study, 300 mM D-arginine exerts a 50% greater destabilization effect than L-arginine (K_{eq} = 0.99 $\pm$ 0.04). Clearly, folding in the TL-TLR tertiary binding motif is capable of kinetically sensing chirality in amino acids, as well as vice versa.

The robustness of such chiral "anti-chaperone" behavior is next probed by examining the unimolecular folding and unfolding rate constants (k_{fold} and k_{unfold}) over a wide range of arginine concentrations. TL-TLR folding and unfolding rate constants are determined by dwell time analysis (Figure 4b)[38] and plotted as a function of [arginine] (Figure 5). In general,
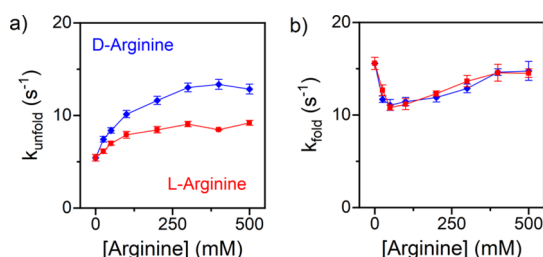

Figure 5. Rate constants for TL-TLR folding (a) and unfolding (b) in the presence of L- and D-arginine. Experiments are carried out in buffer (pH 7.6) with 80 mM background [M$^+$].

the folding rate constants follow qualitatively similar trends for both arginine chiral enantiomers. Specifically, both the D- and L-*folding* rate constants (k_{fold}) decrease modestly (-30%) and then increase ($+30\%$) with respect to [arginine]. By way of contrast, the D- and L-*unfolding* rate constants (k_{unfold}) monotonically increase by nearly 200–300%, which thereby corresponds to a net *destabilization* of the TL-TLR binding motif with increasing [arginine]. Of interest here is a direct comparison between the two chiral enantiomers, for which the *folding* rate constant reveals remarkably little sensitivity to the substrate chirality. Instead, the chiral differences between enantiomers manifest primarily in the *unfolding* rate constant, for which D-arginine is significantly more effective than L-arginine at enhancing the rate.

Thermodynamic Studies of Chirally Sensitive D,L-Arginine-Assisted Unfolding. To probe the thermodynamics of RNA unfolding by the enantiomers of arginine, we turn now to temperature-dependent folding studies. Changes in temperature modify the free energy of folding by the Gibbs expression

$$\Delta G^\circ = \Delta H^\circ - T\Delta S^\circ = -RT\ln(K_{eq}) \qquad (1)$$

where ΔG° is the folding free energy change, ΔH° is the enthalpy of folding, T is the absolute temperature, ΔS° is the entropy of folding, R is the gas constant, and K_{eq} is the folding equilibrium constant. Rearranged into the standard van't Hoff form

$$\ln(K_{eq}) = -\frac{\Delta H^\circ}{R}\left(\frac{1}{T}\right) + \frac{\Delta S^\circ}{R} \qquad (2)$$

a plot of $\ln(K_{eq})$ vs $1/T$ can be used to recover the enthalpy and entropy of folding via linear least-squares analysis. Similarly, an Arrhenius-type expression can be derived from

Kramers' theory for the temperature dependence of rate constants[47,48]

$$\ln(k_{fold/unfold}) = -\frac{\Delta H^\ddagger}{R}\left(\frac{1}{T}\right) + \frac{\Delta S^\ddagger}{R} + \ln(\kappa\nu) \qquad (3)$$

where k is the rate constant, $\Delta H^\ddagger$ and $\Delta S^\ddagger$ are the activation enthalpy and entropy, respectively, ν is the attempt frequency along the reaction coordinate, and κ is the transmission coefficient accounting for deviation from transition state (TS) theory[49] due to diffusive barrier recrossing. The prefactor product $\kappa\nu$ depends on the exact details of the folding energy landscape, but an estimate of $\kappa\nu \sim 10^6$ s^{-1} is plausible from previous studies of RNA and protein folding.[48,50] Furthermore, we note that the thermodynamic entropies ($\Delta S^\ddagger$) obtained from a TS analysis depend only logarithmically on $\kappa\nu$. Thus, the any environmentally induced changes in these TS entropies ($\Delta\Delta S^\ddagger$) remain rigorously independent of this choice of $\kappa\nu$. Nevertheless, caution is indeed warranted when interpreting the absolute intercept values in such Arrhenius plots, as they represent a combination of activation entropy and prefactor contributions.

The results from temperature-dependent experiments (11–27 °C) at a fixed concentration of 100 mM L- and D-arginine are displayed in Figure 6. Consistent with concentration studies, D-arginine is found to decrease TL-TLR stability more than L-arginine (Figure 6a), and the kinetic basis of this chiral-specific destabilization is primarily due to differences in unfolding rather than folding (Figure 6b). Linear regression is applied, and extracted enthalpies and entropies are reported in Table 1. Visual inspection of folding rate constant data (Figure 6b, left panel; see zoomed inset) reveals small but nevertheless clear differences in slopes between enantiomers, indicating that the enthalpic cost to reach the transition state during folding is greater for L-arginine ($\Delta H^\ddagger_{fold}$ 18.9 $\pm$ 2.2 kJ/mol for L-arginine and 11.1 $\pm$ 2.8 kJ/mol for D-arginine). This is intriguing, as no chiral behavior in the folding rate constant was observed in room temperature experiments (Figure 5). The explanation for this is that the difference in activation enthalpy is counteracted by a difference in activation entropy ($\Delta\Delta S^\ddagger_{fold}$ = -26 ± 12 J/(mol K)), which results in a negligibly small net free energy difference at room temperature ($\Delta\Delta G^\ddagger_{fold}$ = $\Delta\Delta H^\ddagger_{fold} - T\Delta\Delta S^\ddagger_{fold}$ = 0.1 $\pm$ 5 kJ/mol). Similarly, the unfolding rate constant (Figure 6b, right panel) appears to exhibit indistinguishable slopes but a clear vertical offset, corresponding to more purely entropic rather than enthalpic contributions to free energies differences between the two enantiomers. However, the data are taken only over a relatively small (<10%) absolute temperature range, with extrapolation resulting in significant correlation between enthalpic (slope) and entropic (intercept) parameters. After careful inclusion of correlated error propagation, the fitted unfolding activation entropies prove to be statistically indistinguishable (174 $\pm$ 3 J/(mol K) for L-arginine and 169 $\pm$ 10 J/(mol K) for D-arginine). Similarly, the van't Hoff thermodynamic parameters (ΔH^0 and ΔS^0) are also found to be identical within experimental error for both 100 mM L- and D-arginine. In order to eliminate the possibility that such agreement is accidental for the chosen arginine concentration, temperature-dependent experiments were also performed at 200 mM arginine but again exhibit no chiral sensitivity (outside of 1σ uncertainties) in the least-squares fits (Figure S1). In summary, temperature-dependent measurements reveal a clear difference
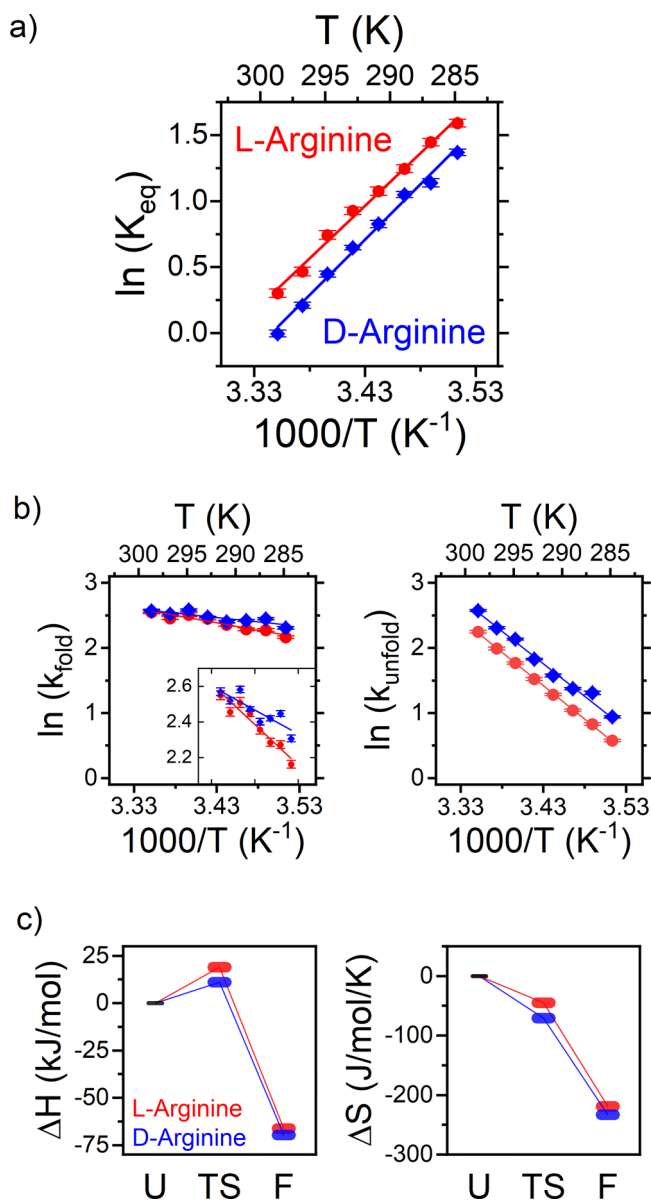
Figure 6. Temperature-dependent studies of folding and unfolding thermodynamics. (a) van't Hoff plot and (b) Arrhenius plots for TL-TLR folding with 100 mM L- and D-arginine. (c) Fitted values for enthalpies (left) and entropies (right) of the folded state (F) and transition state (TS) relative to the unfolded state (U).

our kinetic analysis to additional amino acids (Figure 7). By determining which other amino acids, if any, interact with the
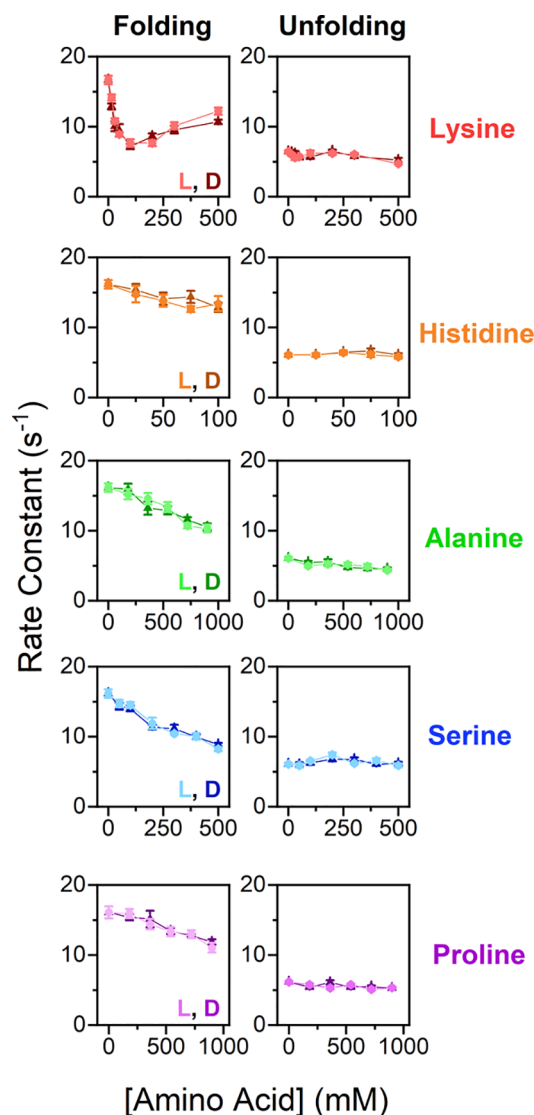

Figure 7. Rate constants for TL-TLR folding (left) and unfolding (right) in the presence of L-amino acids (light symbols) and their D-enantiomers (dark symbols). Concentration ranges for each amino acid are constrained by solubility.

in *folding* activation enthalpies in the presence of L- vs D-arginine, but the thermodynamic basis of chiral differences in *unfolding* activation remains smaller than our experimental resolution.

In Search of Other Amino Acid Chiral Sensitivities in RNA Folding/Unfolding. To provide further insight into the structural origin of such chiral sensitivity, we have extended

TL-TLR construct with chiral specificity, we might glean key molecular characteristics that induce enantiomer-dependent amino acid chaperoning of RNA tertiary folding, namely, whether amino acid side chains are hydrophilic or hydrophobic, charged or uncharged, saturated or unsaturated, and so on. Previous work determined that the TL-TLR fold necessitated amino acid concentrations of order 100 mM to observe significant changes in the folding equilibrium,[15] which

Table 1. Thermodynamic Values from van't Hoff and Arrhenius Analyses for TL-TLR Folding in 100 mmol/L L- vs D-Arginine

	ΔH° (kJ/mol)	$\Delta H^\ddagger_{fold}$ (kJ/mol)	$\Delta H^\ddagger_{unfold}$ (kJ/mol)	ΔS° (J/(mol K))	$\Delta S^\ddagger_{fold}$ (J/(mol K))	$\Delta S^\ddagger_{unfold}$ (J/(mol K))
L-arginine	−66.2(2.2)	18.9(2.2)	85(1)	−219(8)	−45(8)	174(3)
D-arginine	−69.7(2.6)	11.1(2.8)	83(3)	−233(9)	−71(9)	169(10)
	$\Delta\Delta H^\circ$ (kJ/mol)	$\Delta\Delta H^\ddagger_{fold}$ (kJ/mol)	$\Delta\Delta H^\ddagger_{unfold}$ (kJ/mol)	$\Delta\Delta S^\circ$ (J/(mol K))	$\Delta\Delta S^\ddagger_{unfold}$ (J/(mol K))	$\Delta\Delta S^\ddagger_{unfold}$ (J/(mol K))
difference	3(3)	8(4)	2(3)	14(12)	26(12)	5(10)

restricts the present slate of amino acids based on solubility in water.[51] Nevertheless, the set of five soluble amino acids explored herein (lysine, histidine, alanine, serine, and proline) bear side chains with a diverse range of physicochemical properties which cover much of the "amino acid space". By exposing the RNA tertiary fold to this representative suite of five amino acids and their enantiomers, we hope to uncover general structural qualities that give rise to the chiral behavior observed above for arginine.

As a first candidate we consider lysine, which, like arginine, also has a long side chain with a net positive charge, but with an ammonium moiety substituting for the guanidinium group. Despite these physical similarities, little to no chiral dependence between the folding and unfolding rate constants is observed for lysine (see Figure 7, top row). We next examine histidine, whose side chain contains a conjugated hydrocarbon network similar to arginine, but which is predominantly unprotonated (∼2% cationic) under our experimental conditions (pH = 7.6). Again, despite these qualitative similarities, the results reveal no distinction between L- and D-histidine behavior. We additionally investigated amino acids with other side chain types: alanine, with a small and hydrophobic side chain; serine, with a polar hydroxymethyl side chain; and proline, whose amine group is incorporated into an aliphatic heterocycle. The TL-TLR response to each of these amino acids proves to be independent of chirality (Figure 7, rows 3−5). Indeed, among all of the amino acids tested, arginine and arginine alone induces chiral-specific modulation of tertiary folding rates in the TL-TLR construct.

Nevertheless, the different classes of amino acids tested do provide some insight into the salient aspects of arginine's effect on the TL-TLR. First, all amino acids, regardless of side chain, can down-regulate the folding rate. One simple explanation for this is that all amino acids engage in nonspecific binding to the surface of the nucleic acid, such that the *decrease* in surface area upon TL-TLR folding would be thermodynamically disfavored. However, note that not all amino acids have the same effectiveness in this regard; 100 mM histidine, for example, achieves the same degree of slowdown as 500 mM alanine, a 5-fold greater sensitivity. Second, only the positively charged amino acids can, at higher concentrations, *increase* the folding rate. This behavior likely derives from simple ionic shielding of the nucleic acid phosphate backbone by electrolytes, similar to addition of monovalent atomic cations, whereby decreased repulsion between phosphate groups lowers the barrier to folding and increases the folding rate constant.[30,52,53] Finally, and most importantly, arginine is unique in its ability to speed up the rate of *unfolding*. Furthermore, the chiral specific response to arginine is exclusively contained in the unfolding rate constant behavior. Structurally, these data would suggest that arginine's guanidinium-based side chain is responsible its chiral specificity. This is quite curious, however, as the guanidinium group itself is achiral and is 6−7 covalent C−C bonds removed from arginine's chiral center. This immediately raises many intriguing questions, such as how does arginine's chiral carbon affect the binding mode of the arginine molecule, and why does this not occur in the other tested amino acids, which undoubtedly also bind to RNA?

IV. MOLECULAR DYNAMICS SIMULATIONS

To provide insight into the mechanistic origin of such a chiral sensitivity to amino acid-assisted RNA folding/unfolding, we have additionally performed computational modeling of the interactions between the TL-TLR single molecule construct and the two chiral enantiomers of arginine. At the outset, we first considered a "molecular docking" strategy,[54] for which a variety of candidate ligand-macromolecule binding "poses" are heuristically generated and scored to predict binding affinities to specific binding pockets. However, the use of molecular docking to predict relative binding free energies of enantiomeric pairs has been shown to be insufficiently reliable.[55] Therefore, the molecular docking approach was not selected for these studies. Instead, we choose to employ all-atom, explicit solvent molecular dynamics (MD)[56,57] as our computational strategy for assessing amino acid binding to the TL-TLR fold, exploiting well-tested computational tools such as Nanoscale Molecular Dynamics (NAMD) and Visual Molecular Dynamics (VMD) for MD simulation as parallel *in silico* experiments. The key limitation of such calculations is the simulation time scale, which for the present construct sizes is typically <10 μs, though longer run times can in principle be accessed with enhanced sampling methods[56,58] or coarse-grained models.[59,60] However, as the TL-TLR construct used in these studies folds on the 10−100 ms time scale, efforts to simulate the full equilibrium dynamics of TL-TLR tertiary folding in real time would be computationally prohibitive. We instead take a conceptually simpler approach, performing three separate shorter time scale simulations with which to evaluate arginine distributions in equilibrium with each of the TL-TLR components. Specifically, we run three NPT simulations in parallel for 100 ns, probing L- and D-arginine attachment onto (i) the GAAA tetraloop (initial structure: PDB 1ZIF), (ii) the 11-nt tetraloop receptor (initial structure: PDB 1TLR), and (iii) the docked tetraloop−tetraloop receptor contained in the P4−P6 domain of the *Tetrahymena thermophilia* intron (initial structure: PDB 1GID, truncated to TL-TLR residues; see Methods section). Each of the three initial TL, TLR, and TL-TLR structures is placed in a water box with periodic boundary conditions and appropriate potassium and chloride ion densities to mimic ionic strength values used experimentally, plus 100 mM of either L- or D-arginine (Figure 8; see Methods section for details). In effect, this piecewise strategy serves to model arginine interaction with the TL-TLR in the vicinity of its folding and unfolding free energy minima, which circumvents the need for ultralong simulation time scales. The corresponding penalty is being unable to observe the folding transition state, which limits dynamical interpretation. Never-
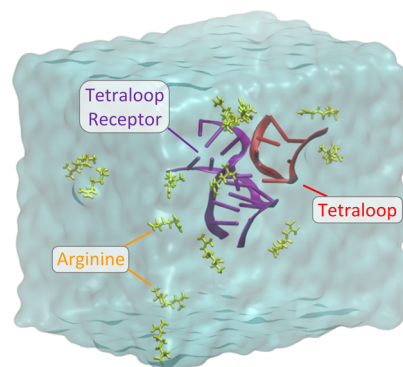

Figure 8. All-atom, explicit solvent simulation of arginine condensation onto the TL-TLR system. Simulations consist of nucleic acid (docked TL-TLR shown; TL in red, TLR in purple) solvated in TIP3P water with 100 mM L/D-arginine (yellow).

theless, these MD simulations offer first insights into the thermodynamics of the overall folding process.

As the first step in our analysis, we evaluate the interaction energy between the three nucleic acid constructs and their surrounding arginine ions. Free energies corresponding to individual snapshots 200 ps apart for each of the MD trajectories are calculated by the molecular mechanics Poisson–Boltzmann surface area (MMPBSA) method.[61] In MMPBSA, the binding free energy ΔG_{bind} is computed by combining the change in three energy contributions upon ligand binding:

$$\Delta G_{bind} = \Delta E_{MM} + \Delta G_{solv,PB} + \Delta G_{solv,SA} \tag{4}$$

In this expression, E_{MM} is molecular mechanics force field energy, $G_{solv,PB}$ is the solvation free energy under a Poisson–Boltzmann treatment, and $G_{solv,SA}$ is a semiempirical term accounting for the free energy of the solute–solvent interface and assumed proportional to surface area. One important caveat to the use of MMPBSA is that the entropic contribution to the binding free energy is incomplete. Specifically, the ligand–receptor conformational entropy change (ΔS_{conf}) is unaccounted for and cannot be rigorously incorporated. While there are a number of approximate methods for calculating ΔS_{conf}, in practice such computations fail to improve the accuracy and thus are not included in our estimates of ΔG_{bind}.[61] Despite such potential concerns, MMPBSA has previously been shown to accurately reproduce experimental relative binding free energies of enantiomer pairs,[62,63] motivating its use here.

These MMPBSA computations reveal two important features for arginine binding onto the single molecule nucleic acid construct. First, as depicted in Figure S2, the MMPBSA energies exhibit an initial, fast relaxation of $t_{relax} \sim 10$ ns, with an additional longer time scale relaxation which goes beyond our simulation time limits. The fast relaxation agrees reasonably well with the predicted diffusion times for arginine to reach to the surface of the nucleic acid ($\tau_{diffusion} \sim R^2/D \sim$ 13 ns), based on the typical distance between the arginine and nucleic acid ($R \sim 30$ Å) and the diffusion coefficient of arginine in water ($D = 80 \ \mu m^2/s$).[64] Energetic relaxation appears to converge most quickly for the smallest simulated system, the lone tetraloop (TL). On the other hand, the TLR and docked TL-TLR constructs do not reach full equilibration after 100 ns, with arginine molecules continuing to explore a variety of binding poses, some more favorable than others. Even if we provide an additional +100 ns to the simulation, the TL-TLR construct still does not reach the equilibrium ergodic limit. It is not surprising that the binding free energies are not yet fully converged in ~200 ns, as small molecule docking to specific binding sites can take multiple microseconds to occur.[56,57]

Second, and of primary importance, the MD simulations reveal that MMPBSA energies of arginine interactions with nucleic acids to be both D,L-enantiomer- and folding-state-specific. In particular, the MMPBSA energies computed for L- and D-arginine interactions with (i) TL, (ii) TLR, and (iii) the docked TL-TLR are plotted as a histogram in Figure 9. The MD simulations indicate only marginal differences in the binding affinities of L- and D-arginine to the TL ($\Delta\Delta G_{bind} = \Delta G_{bind,D-Arg} - \Delta G_{bind,L-Arg} = -1.3 \pm 1.9$ kJ/mol) and TLR ($\Delta\Delta G_{bind} = +1.6 \pm 4.1$ kJ/mol). The sum in the two chiral free energy differences is therefore $\Delta\Delta G_{bind,unfolded} = 0.3 \pm 4.5$, which is zero within the simulation uncertainties. However, for
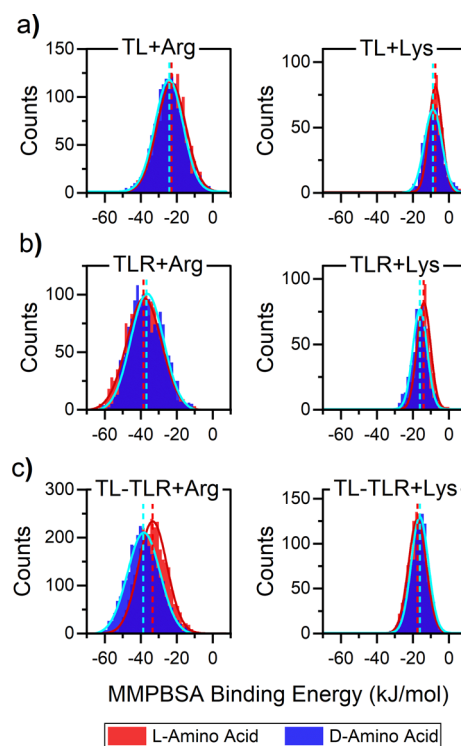

Figure 9. Histogram of MMPBSA-computed binding free energies for L- and D-enantiomers of arginine (left) and lysine (right) with (a) the undocked TL, (b) the undocked TLR, and (c) the docked TL-TLR. Solid curves are Gaussian fits, and vertical dashed lines are histogram centers.

the docked TL-TLR simulation, there is a much larger difference in binding energies for L- and D-arginine, favoring D-arginine by $\Delta\Delta G_{bind,folded} = -5.3 \pm 3.4$ kJ/mol.

To better appreciate both the statistical significance and uncertainties of these chirally sensitive results, we have explored identical MD simulations with D/L-lysine in place of D/L-arginine (Figure 9, right panels). In particular, recall that lysine experimentally exhibits no chirally specific behavior in excess of the uncertainty limit (Figure 7), from which we would expect to see statistically vanishing chiral sensitivity in the molecular dynamics simulations. In terms of absolute magnitudes, we find that lysine displays ~2-fold smaller binding free energies than arginine, with chirally dependent differences only on the order of 1–2 kJ/mol ($\Delta\Delta G_{bind}(TL) =$ +1.3 kJ/mol, $\Delta\Delta G_{bind}(TLR) = +2.1$ kJ/mol, and $\Delta\Delta G_{bind}(TL-TLR) = -1.4$ kJ/mol). Indeed, from these values we can estimate roughly that the computational measurement uncertainties are on the same 1–2 kJ/mol order. Most importantly, we can conclude that arginine binding to the unfolded construct components (TL and TLR) is chirally insensitive within our MMPBSA uncertainties, whereas arginine binding to the fully folded TL-TLR shows a distinct preference for D- vs L-arginine.

We can take these MD simulations one step further in an effort to identify the spatial region of preferred attachment for chiral D- vs L-arginine. To do this, 3D probability distributions of the arginine atoms $p(x,y,z)$ are computed by aligning MD trajectories and binning arginine atom locations using a 0.5 Å grid spacing. In the equilibrium thermodynamic limit, these probabilities can be converted into a 3D free energy distribution $\Delta G(x,y,z)$ via[65]

$$\Delta G(x, y, z) = -k_B T \ln\left(\frac{p(x, y, z)}{p_0}\right) \tag{5}$$

where p_0 is the bulk concentration at the periphery of the simulation cell, as determined by the asymptotic value of the arginine−RNA radial distribution function (Figure S3). By way of example, the resulting two free energy isosurfaces for L- and D-arginine binding to the docked TL-TLR construct are plotted in Figure 10, corresponding to a relatively strong
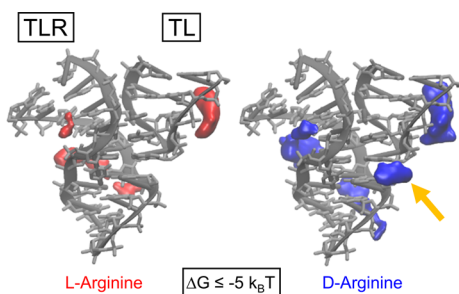

Figure 10. Free energy isosurfaces ($\Delta G \leq -5 \; k_B T$) for arginine binding to the docked TL-TLR structure. Arrow indicates the presence of an arginine-binding pocket preferential for the D- vs L-enantiomer at the interface of TL and TLR. For other perspectives and free energy isosurfaces, see the Supporting Information.

binding slice at $\Delta G = -12$ kJ/mol and therefore revealing the most significantly occupied binding pockets. (We note that many weaker and stronger binding locations exist across the full surface of the nucleic acid. For a full 3D view, including isosurfaces for other binding pocket depths and nucleic acids, see Movies S1−S3). Interestingly, most of these binding pockets are shared relatively equally by both L- and D-arginine. However, there is at least one notably large region at the cleft interface between the TL and TLR constructs to which D-arginine binds with significantly greater propensity than L-arginine, as identified with an arrow in Figure 10. Most importantly, MD simulations for the undocked TL and TLR, by way of contrast, show no binding pockets with chiral preference for L- or D-arginine (as evident in Movies S1 and S2). Furthermore, for parallel MD simulations with lysine binding, no chirally specific binding pockets are observed for any of the TL, TLR, and TL-TLR constructs simulated systems (Movies S4−S6), consistent with the complete lack of chiral sensitivity observed experimentally in amino acid induced folding/unfolding. Thus, although these simulations are run only for 100−200 ns and therefore do not fully sample the true equilibrium state, these MD trajectories do already reveal chiral enantiomer-specific binding interactions on the submicrosecond time scale, qualitatively consistent with our single molecule experimental results. It is of course possible that even longer MD simulations would provide additional examples of stereospecific binding of arginine to this TL-TLR tertiary folding motif.

V. DISCUSSION

This paper speculates that homochirality may have been transmitted to amino acids from RNA through chiral differences in amino acid-based modification of RNA folding behavior. To help assess such a conjecture, we have used single-molecule FRET measurements coupled with all-atom MD simulations, focusing on the 11-nt GAAA tetraloop−

tetraloop receptor as a model RNA tertiary fold. The TL-TLR folding/unfolding of this tertiary motif is found to clearly depend on amino acid chirality for arginine (Figure 5), with only negligible sensitivities exhibited for each of the other classes (hydrophobic/hydrophilic, charged/uncharged, and saturated/unsaturated) of the six amino acids investigated (Figure 7). Outside of simple empirical observation, the question remains: how does the chiral nature of D- vs L-arginine influence its interaction with the TL-TLR tertiary binding motif, and why might structurally similar amino acids not also exhibit a similarly strong chiral effect? We examine the evidence for relevant clues.

First, the concentration-dependent data (Figures 5 and 7) reveal that arginine is unique among the six amino acids tested, specifically impacting the rate constant for TL-TLR *unfolding*, and indeed, buried therein lies all chiral dependence. Each of the other amino acids tested modify the folding rates but have only minimal effect on the unfolding rates. Lysine even shares arginine's nonmonotonic influence on the folding rate constant, likely due to positive charge shielding effects, but only in the presence of arginine does the TL-TLR *unfolding* rate constant change significantly, specifically increasing from $k_{unfold} = 5.4 \pm 0.4$ to $8.0 \pm 0.4 \; s^{-1}$ with 100 mM L-arginine. Furthermore, such clear TL-TLR sensitivity to arginine chirality is manifested exclusively in the unfolding process, with D-arginine accelerating the unfolding rate constant by 50% more than L-arginine at 100 mM. This suggests a connection between arginine's special ability to enhance TL-TLR unfolding and its chiral-specific influence. Molecular dynamics (MD) simulations strongly support this connection, as any differential L- vs D-arginine binding to the TL and TLR constructs is only observed in the folded (TL-TLR) state, whereas the unfolded state would appear to bind both enantiomers of arginine equivalently.

Second, results from temperature-dependent experiments reveal small but significant differences between the folding activation enthalpy of the TL-TLR motif with L- vs D-arginine, with $\Delta\Delta H^{\ddagger}_{fold}$ (D- vs L-) = 8 ± 4 kJ/mol in favor of the D-enantiomer. The differential binding of arginine to the folding, unfolding, and transition states results in changes in the relative free energies of these states, with greater binding leading to greater free energy stabilization. Therefore, the chiral difference in activation enthalpy could be due to either preferential binding of D-arginine to the transition state of the TL-TLR or superior L-arginine binding to the unfolded state, or a combination of the two. As the MMPBSA calculations suggest that each enantiomer of arginine binds equivalently to the separated TL and TLR constructs, the more consistent explanation would seem to be that D-arginine binds to the TL-TLR folding transition state more favorably than L-arginine, thereby reducing the activation enthalpy for folding. It is worth noting that this reduced activation enthalpy is almost exactly compensated by an additional entropy cost ($\Delta\Delta S^{\ddagger}_{fold} = -26 \pm 12 \; J/(mol \; K)$, raising the free energy barrier for D-arginine), presumably due to the loss of translational and conformational entropy with one or more arginine molecules binding. This results in vanishingly small differences in activation free energies ($\Delta\Delta G^{\ddagger}_{fold} = \Delta\Delta H^{\ddagger}_{fold} - T\Delta\Delta S^{\ddagger}_{fold}$) at room temperature, and therefore the *folding* rate constants for L- and D-arginine become largely indistinguishable. Less can be inferred about the unfolding process from temperature-dependent experiments, as the measured thermodynamic parameters for L- and D-arginine are within

experimental uncertainty ($\Delta\Delta H^{\ddagger}_{unfold} < 3$ kJ/mol, $\Delta\Delta S^{\ddagger}_{unfold} < 10$ J/(mol K)). That the thermodynamic differences are modest is not surprising; D-arginine's 30% faster unfolding rate constant k_{unfold} at 100 mM would from transition state theory require a difference in activation free energy, $\Delta\Delta G^{\ddagger} = 0.6$ kJ/mol, which is relatively small compared to the thermal energy product $k_B T = 2.4$ kJ/mol.

Our MD simulations have revealed that TL and TLR docking creates an interstitial cleft to which D-arginine binds more effectively than L-arginine. However, it must be the case that these simulations cannot fully explore all binding interactions, as a prediction of greater D-arginine stabilization of the folded state from MD would be in direct contradiction with the experimental results, for which we find that destabilization of the TL-TLR is found to be greater for D-arginine than L-arginine. One possible reason for such a discrepancy is the limited simulation time (100 ns) explored, which prevents the system from surmounting large kinetic barriers, for instance, arginine displacement of a tightly bound potassium ion or large structural rearrangements in the nucleic acid. Presumably, at longer time scales an additional binding pocket preferential to L-arginine would emerge, and therefore long simulations and/or enhanced sampling techniques are necessary to resolve the ultimate cause of greater destabilization of the TL-TLR fold by D-arginine. Nevertheless, it is interesting that even relatively weak transient binding can display strong chiral preferences, an observation which we might expect to be generalizable to other RNA−ligand systems. Furthermore, the fact that the chirality-sensitive binding pocket is localized at the interface of the TL and TLR suggests that RNA tertiary interfaces in general might hold the conformational key to generating such enantiospecific behavior.

MD simulations suggest that arginine's positive charge in combination with its side chain's especially strong interactions with nucleic acids is responsible for its special ability to modulate TL-TLR folding in a chiral specific fashion. Because of the cationic nature of the arginine residue, it readily participates in the anionic atmosphere of the nucleic acid.[66] Indeed, the arginine−nucleic acid radial distribution function (Figure S3) shows that arginine concentration near nucleic acids is enhanced by 10−25-fold over the bulk concentration. One might therefore expect such large local concentrations to enable arginine to sample weak, chirality-specific binding sites inaccessible to neutral or negatively charged amino acids. With its positively charged amide side chain, lysine would also be expected to experience a similar increase in local ion atmosphere near the polyanionic backbone. However, the present MMPBSA calculations suggest and are at least consistent with the lysine side chain having a greatly reduced ability for binding to RNA than the guanidinium cation group in arginine.

The primary motivation of this study is to investigate a potential mechanism by which nucleic acid chirality was imprinted upon amino acids, and a few remarks on the evolutionary implications of these results are appropriate. In the hypothesis considered here, the role of amino acids in early biology was to promote correct RNA folding, perhaps by destabilizing misfolded states. This is similar to the role of modern chaperone proteins, which unfold misfolded proteins to allow them a second chance to fold correctly. The L-amino acids may have acted as superior chaperones to D-amino acids, leading to increased fitness for cells containing an enantiomeric

excess of L-amino acids, which would drive evolution toward homochiral synthesis of L-amino acids. In our experiments, only one amino acid, arginine, is found to exhibit chiral-specific chaperone properties, while all other tested amino acids modify RNA folding independent of chirality. This casts doubt on the chaperone-homochirality hypothesis, as it seems unlikely that a single amino acid's interaction with RNA would drive synthesis of all amino acids to L-chirality. Furthermore, arginine is usually considered to have been a late arrival to the amino acid alphabet, based on its low prebiotic availability.[67] However, prebiotic availability may not be an appropriate criterion for the development of the genetic code, and recently Blanco et al. have highlighted arginine as a likely candidate for an early amino acid based on RNA−protein binding.[68] If arginine or another biophysically related amino acid was highly enriched in ancient biology, then the chiral sensitivity observed in these studies may have been significant enough to steer evolution toward L-amino acids.

VI. CONCLUSION

Single molecule experiments have been used to explore the potential sensitivity of RNA tertiary folding rate constants and equilibria to amino acid chirality. Of the four classes of amino acids studied, only arginine exhibits any chiral-specific influence on the RNA folding equilibrium for the TL-TLR. Both enantiomers of arginine increase the unfolding rates and thereby destabilize the RNA, but the non-natural enantiomer (D-arginine) is found to be more strongly destabilizing, by up to a factor of 50% difference in equilibrium constant at 300 mM. Kinetically the source of this effect is exclusively rooted in changes the unfolding rate constant, with essentially no measurable difference in the corresponding folding rate constant with D- vs L-arginine chirality. From temperature-dependent studies of the rate constants, these chiral sensitivities can be traced back to simple thermodynamical variables, specifically with a reduced activation enthalpy for folding ($\Delta\Delta H^{\ddagger} = 8 \pm 4$ kJ/mol) in the presence of D-arginine. In order to obtain additional preliminary insights into the mechanism for such chiral sensitivity, we have explored molecular dynamics (MD) simulations for the folding and unfolding events with NAMD and VMD computer platforms, specifically by using 100 ns long trajectories to discover chirally sensitive free energy differences in D- vs L-arginine binding to the TL, TLR, and TL-TLR constructs. Interestingly, the results indicate a complete lack of chiral sensitivity to the unfolded TL and TLR species, but with a clear differential chiral effect on D- vs L-arginine binding to the fully folded TL-TLR construct. Furthermore, the probability distributions from the MD simulations have been used to generate a 3D free energy landscape for binding of D- and L-arginine to the folded TL-TLR tertiary motif, revealing that RNA−RNA tertiary interfaces may provide a more general source of chirality-sensing binding pockets for enhanced D- vs L-arginine attachment. These preliminary computational results corroborate many but not all of the chiral experimental findings, offering first insights into support of a putative mechanism for RNA chirality influencing and being influenced by associated amino acid chirality.

■ ASSOCIATED CONTENT

Ⓢ Supporting Information

The Supporting Information is available free of charge at https://pubs.acs.org/doi/10.1021/acs.jpcb.0c07420.

Arrhenius results at 200 mM arginine, MMPBSA energy trajectories, and sample radial distribution function (PDF)

Movie S1 (MPG)
Movie S2 (MPG)
Movie S3 (MPG)
Movie S4 (MPG)
Movie S5 (MPG)
Movie S6 (MPG)

■ AUTHOR INFORMATION

Corresponding Author

David J. Nesbitt — *JILA, National Institute of Standards and Technology and University of Colorado Boulder, Boulder, Colorado 80309, United States; Department of Chemistry and Department of Physics, University of Colorado Boulder, Boulder, Colorado 80309, United States;* ● orcid.org/0000-0001-5365-1120; Email: djn@jila.colorado.edu

Authors

David A. Nicholson — *JILA, National Institute of Standards and Technology and University of Colorado Boulder, Boulder, Colorado 80309, United States; Department of Chemistry, University of Colorado Boulder, Boulder, Colorado 80309, United States*

Abhigyan Sengupta — *Department of Physics, Technical University of Munich, Munich, Germany 85748*

Complete contact information is available at:
https://pubs.acs.org/10.1021/acs.jpcb.0c07420

Notes

The authors declare no competing financial interest.

■ REFERENCES

(1) Blackmond, D. G. The origin of biological homochirality. *Cold Spring Harbor Perspect. Biol.* **2010**, *2* (5), No. a002147.

(2) Zask, A.; Ellestad, G. Biomimetic syntheses of racemic natural products. *Chirality* **2018**, *30* (2), 157–164.

(3) Finefield, J. M.; Sherman, D. H.; Kreitman, M.; Williams, R. M. Enantiomeric natural products: occurrence and biogenesis. *Angew. Chem., Int. Ed.* **2012**, *51* (20), 4802–4836.

(4) Banik, S. D.; Nandi, N. Chirality and protein biosynthesis. In *Biochirality: Origins, Evolution and Molecular Recognition*; Cintas, P., Ed.; Springer: Heidelberg, 2013; pp 255–305.

(5) Genchi, G. An overview on D-amino acids. *Amino Acids* **2017**, *49* (9), 1521–1533.

(6) Joyce, G. F. The antiquity of RNA-based evolution. *Nature* **2002**, *418* (6894), 214–21.

(7) Tamura, K.; Schimmel, P. Chiral-selective aminoacylation of an RNA minihelix. *Science (Washington, DC, U. S.)* **2004**, *305* (5688), 1253.

(8) Tamura, K. Molecular basis for chiral selection in RNA aminoacylation. *Int. J. Mol. Sci.* **2011**, *12*, 4745–4757.

(9) Herschlag, D. RNA chaperones and the RNA folding problem. *J. Biol. Chem.* **1995**, *270*, 20871–20874.

(10) Woodson, S. A. Taming free energy landscapes with RNA chaperones. *RNA Biol.* **2010**, *7* (6), 677–86.

(11) Chen, S. J. RNA folding: conformational statistics, folding kinetics, and ion electrostatics. *Annu. Rev. Biophys.* **2008**, *37*, 197–214.

(12) Saibil, H. Chaperone machines for protein folding, unfolding and disaggregation. *Nat. Rev. Mol. Cell Biol.* **2013**, *14* (10), 630–642.

(13) Arakawa, T.; Timasheff, S. N. The stabilization of proteins by osmolytes. *Biophys. J.* **1985**, *47* (3), 411–414.

(14) Nicholson, D. A.; Sengupta, A.; Sung, H.-L.; Nesbitt, D. J. Amino acid stabilization of nucleic acid secondary structure: kinetic insights from single-molecule studies. *J. Phys. Chem. B* **2018**, *122* (43), 9869–9876.

(15) Sengupta, A.; Sung, H. L.; Nesbitt, D. J. Amino acid specific effects on rna tertiary interactions: single-molecule kinetic and thermodynamic studies. *J. Phys. Chem. B* **2016**, *120*, 10615–10627.

(16) Yarus, M. A specific amino acid binding site composed of RNA. *Science (Washington, DC, U. S.)* **1988**, *240* (4860), 1751–8.

(17) Burg, M. B.; Ferraris, J. D. Intracellular organic osmolytes: function and regulation. *J. Biol. Chem.* **2008**, *283* (12), 7309–7313.

(18) Khan, S. H.; Ahmad, N.; Ahmad, F.; Kumar, R. Naturally occurring organic osmolytes: from cell physiology to disease prevention. *IUBMB Life* **2010**, *62* (12), 891–895.

(19) Ando, T.; Takahashi, S.; Tamura, K. Principles of chemical geometry underlying chiral selectivity in RNA minihelix aminoacylation. *Nucleic Acids Res.* **2018**, *46* (21), 11144–11152.

(20) Tamura, K. RNA-directed molecular asymmetry of amino acids. *Viva Origino* **2010**, *38* (4), 18–22.

(21) Illangasekare, M.; Yarus, M. Phenylalanine-binding RNAs and genetic code evolution. *J. Mol. Evol.* **2002**, *54* (3), 298–311.

(22) Yarus, M. Amino acids as RNA ligands: a direct-RNA-template theory for the code's origin. *J. Mol. Evol.* **1998**, *47* (1), 109–117.

(23) Yarus, M. RNA-ligand chemistry: a testable source for the genetic code. *RNA* **2000**, *6* (4), 475–484.

(24) Illangasekare, M.; Turk, R.; Peterson, G. C.; Lladser, M.; Yarus, M. Chiral histidine selection by D-ribose RNA. *RNA* **2010**, *16* (12), 2370–2383.

(25) Tohala, L.; Oukacine, F.; Ravelet, C.; Peyrin, E. Chiral resolution capabilities of DNA oligonucleotides. *Anal. Chem.* **2015**, *87* (11), 5491–5495.

(26) Sivaleela, T.; Kumar, M. R.; Prabhakar, S.; Bhaskar, G.; Vairamani, M. Chiral discrimination of α-amino acids by DNA tetranucleotides under electrospray ionization conditions. *Rapid Commun. Mass Spectrom.* **2008**, *22* (2), 204–210.

(27) Yarus, M.; Majerfeld, I. Co-optimization of ribozyme substrate stacking and L-arginine binding. *J. Mol. Biol.* **1992**, *225* (4), 945–9.

(28) Holmstrom, E. D.; Nesbitt, D. J. Biophysical Insights from Temperature-Dependent Single-Molecule Forster Resonance Energy Transfer. *Annu. Rev. Phys. Chem.* **2016**, *67*, 441–65.

(29) Fiore, J. L.; Nesbitt, D. J. An RNA folding motif: GNRA tetraloop-receptor interactions. *Q. Rev. Biophys.* **2013**, *46* (3), 223–64.

(30) Downey, C. D.; Fiore, J. L.; Stoddard, C. D.; Hodak, J. H.; Nesbitt, D. J.; Pardi, A. Metal ion dependence, thermodynamics, and kinetics for intramolecular docking of a GAAA tetraloop and receptor connected by a flexible linker. *Biochemistry* **2006**, *45*, 3664–3673.

(31) Seol, Y.; Skinner, G. M.; Visscher, K.; Buhot, A.; Halperin, A. Stretching of homopolymeric RNA reveals single-stranded helices and base-stacking. *Phys. Rev. Lett.* **2007**, *98* (15), 158103.

(32) Roy, R.; Hohng, S.; Ha, T. A practical guide to single-molecule FRET. *Nat. Methods* **2008**, *5* (6), 507–16.

(33) Smith, C. L.; Milea, J. S.; Nguyen, G. H. Immobilization of nucleic acids using biotin-strept(avidin) systems. In *Immobilisation of DNA on Chips II*; Wittmann, C., Ed.; Springer: Berlin, 2005; pp 63–90.

(34) Aitken, C. E.; Marshall, R. A.; Puglisi, J. D. An oxygen scavenging system for improvement of dye stability in single-molecule fluorescence experiments. *Biophys. J.* **2008**, *94* (5), 1826−35.

(35) Axelrod, D. Total internal reflection fluorescence microscopy. In *Methods in Cell Biology*, 1st ed.; Elsevier: 2008; Vol. *89*, pp 169−221.

(36) Mullikin, J. C.; van Vliet, L. J.; Netten, H.; Boddeke, F. R.; van der Feltz, G.; Young, I. T. *Methods for CCD Camera Characterization*; SPIE: 1994; Vol. *2173*.

(37) Cohen, E. A. K.; Ober, R. J. Image registration error analysis with applications in single molecule microscopy. *In 2012 9th IEEE International Symposium on Biomedical Imaging (ISBI)* **2012**, 996−999.

(38) Hodak, J. H.; Fiore, J. L.; Nesbitt, D. J.; Downey, C. D.; Pardi, A. Docking kinetics and equilibrium of a GAAA tetraloop-receptor motif probed by single-molecule FRET. *Proc. Natl. Acad. Sci. U. S. A.* **2005**, *102* (30), 10505.

(39) Case, D. A.; Belfon, K.; Ben-Shalom, I. Y.; Brozell, S. R.; Cerutti, T. E.; Cheatham, III, V. W. D.; Cruzeiro, T. A.; Darden, R. E.; Duke, D. G.; Giambasu, G.; et al. *AMBER 2019*; University of California, San Francisco, 2019.

(40) Mark, P.; Nilsson, L. Structure and dynamics of the TIP3P, SPC, and SPC/E water models at 298 K. *J. Phys. Chem. A* **2001**, *105* (43), 9954−9960.

(41) Humphrey, W.; Dalke, A.; Schulten, K. VMD: visual molecular dynamics. *J. Mol. Graphics* **1996**, *14* (1), 33−38.

(42) Zgarbova, M.; Otyepka, M.; Sponer, J.; Mladek, A.; Banas, P.; Cheatham, T. E., III; Jurecka, P. Refinement of the Cornell et al. nucleic acids force field based on reference quantum chemical calculations of glycosidic torsion profiles. *J. Chem. Theory Comput.* **2011**, *7* (9), 2886−2902.

(43) Joung, I. S.; Cheatham, T. E., III Determination of alkali and halide monovalent ion parameters for use in explicitly solvated biomolecular simulations. *J. Phys. Chem. B* **2008**, *112* (30), 9020−41.

(44) Horn, A. H. A consistent force field parameter set for zwitterionic amino acid residues. *J. Mol. Model.* **2014**, *20* (11), 2478.

(45) Phillips, J. C.; Braun, R.; Wang, W.; Gumbart, J.; Tajkhorshid, E.; Villa, E.; Chipot, C.; Skeel, R. D.; Kalé, L.; Schulten, K. Scalable molecular dynamics with NAMD. *J. Comput. Chem.* **2005**, *26* (16), 1781−1802.

(46) Stone, J. E. An efficient library for parallel ray tracing and animation. Master's Thesis, University of Missouri, Rolla, 1998.

(47) Dupuis, N. F.; Holmstrom, E. D.; Nesbitt, D. J. Tests of Kramers' theory at the single-molecule level: evidence for folding of an isolated RNA tertiary interaction at the viscous speed limit. *J. Phys. Chem. B* **2018**, *122* (38), 8796−8804.

(48) Hori, N.; Denesyuk, N. A.; Thirumalai, D. Frictional effects on RNA folding: speed limit and Kramers turnover. *J. Phys. Chem. B* **2018**, *122* (49), 11279−11288.

(49) Laidler, K. J.; King, M. C. Development of transition-state theory. *J. Phys. Chem.* **1983**, *87* (15), 2657−2664.

(50) Best, R. B.; Hummer, G. Diffusive model of protein folding dynamics with Kramers turnover in rate. *Phys. Rev. Lett.* **2006**, *96* (22), 228104.

(51) Amend, J. P.; Helgeson, H. C. Solubilities of the common L-α-amino acids as a function of temperature and solution pH. *Pure Appl. Chem.* **1997**, *69* (5), 935−942.

(52) Bisaria, N.; Herschlag, D. Probing the kinetic and thermodynamic consequences of the tetraloop/tetraloop receptor monovalent ion-binding site in P4-P6 RNA by smFRET. *Biochem. Soc. Trans.* **2015**, *43* (2), 172−8.

(53) Holmstrom, E. D.; Fiore, J. L.; Nesbitt, D. J. Thermodynamic origins of monovalent facilitated RNA folding. *Biochemistry* **2012**, *51* (18), 3732−43.

(54) Meng, X. Y.; Zhang, H. X.; Mezei, M.; Cui, M. Molecular docking: a powerful approach for structure-based drug discovery. *Curr. Comput.-Aided Drug Des.* **2011**, *7* (2), 146−57.

(55) Ramírez, D.; Caballero, J. Is it reliable to use common molecular docking methods for comparing the binding affinities of enantiomer pairs for their protein target? *Int. J. Mol. Sci.* **2016**, *17* (4), 525.

(56) Sponer, J.; Bussi, G.; Krepl, M.; Banas, P.; Bottaro, S.; Cunha, R. A.; Gil-Ley, A.; Pinamonti, G.; Poblete, S.; Jurecka, P.; Walter, N. G.; Otyepka, M. RNA structural dynamics as captured by molecular simulations: a comprehensive overview. *Chem. Rev.* **2018**, *118* (8), 4177−4338.

(57) Sponer, J.; Banas, P.; Jurecka, P.; Zgarbova, M.; Kuhrova, P.; Havrila, M.; Krepl, M.; Stadlbauer, P.; Otyepka, M. Molecular dynamics simulations of nucleic acids. From tetranucleotides to the ribosome. *J. Phys. Chem. Lett.* **2014**, *5* (10), 1771−82.

(58) Mlynsky, V.; Bussi, G. Exploring RNA structure and dynamics through enhanced sampling simulations. *Curr. Opin. Struct. Biol.* **2018**, *49*, 63−71.

(59) Hyeon, C.; Thirumalai, D. Capturing the essence of folding and functions of biomolecules using coarse-grained models. *Nat. Commun.* **2011**, *2*, 487.

(60) Jonikas, M. A.; Radmer, R. J.; Laederach, A.; Das, R.; Pearlman, S.; Herschlag, D.; Altman, R. B. Coarse-grained modeling of large RNA molecules with knowledge-based potentials and structural filters. *RNA* **2009**, *15* (2), 189−199.

(61) Genheden, S.; Ryde, U. The MM/PBSA and MM/GBSA methods to estimate ligand-binding affinities. *Expert Opin. Drug Discovery* **2015**, *10* (5), 449−461.

(62) Kocakaya, S. O.; Turgut, Y.; Pirinççioglu, N. Enantiomeric discrimination of chiral organic salts by chiral aza-15-crown-5 ether with C1 symmetry: experimental and theoretical approaches. *J. Mol. Model.* **2015**, *21* (3), 55.

(63) Choi, Y.; Jung, S. Molecular dynamics (MD) simulations for the prediction of chiral discrimination of N-acetylphenylalanine enantiomers by cyclomaltoheptaose (β-cyclodextrin, β-CD) based on the MM−PBSA (molecular mechanics−Poisson−Boltzmann surface area) approach. *Carbohydr. Res.* **2004**, *339* (11), 1961−1966.

(64) Wu, Y.; Ma, P.; Liu, Y.; Li, S. Diffusion coefficients of L-proline, L-threonine and L-arginine in aqueous solutions at 25°C. *Fluid Phase Equilib.* **2001**, *186* (1), 27−38.

(65) Chen, A. A.; Draper, D. E.; Pappu, R. V. Molecular simulation studies of monovalent counterion-mediated interactions in a model RNA kissing loop. *J. Mol. Biol.* **2009**, *390* (4), 805−819.

(66) Lipfert, J.; Doniach, S.; Das, R.; Herschlag, D. Understanding nucleic acid-ion interactions. *Annu. Rev. Biochem.* **2014**, *83*, 813−41.

(67) Trifonov, E. N. Consensus temporal order of amino acids and evolution of the triplet code. *Gene* **2000**, *261* (1), 139−51.

(68) Blanco, C.; Bayas, M.; Yan, F.; Chen, I. A. Analysis of evolutionarily independent protein-RNA complexes yields a criterion to evaluate the relevance of prebiotic scenarios. *Curr. Biol.* **2018**, *28* (4), 526−537.